Physics Letters B 677 (2009) 139–144

Contents lists available at ScienceDirect

Physics Letters B

www.elsevier.com/locate/physletb

Resonant breakup of ^{6}Li by ^{209}Bi

S. Santra *, V.V. Parkar, K. Ramachandran, U.K. Pal, A. Shrivastava, B.J. Roy, B.K. Nayak, A. Chatterjee, R.K. Choudhury, S. Kailas

Nuclear Physics Division, Bhabha Atomic Research Centre, Mumbai 400085, India

ARTICLE INFO

Article history:
Received 17 October 2008
Received in revised form 6 April 2009
Accepted 10 May 2009
Available online 14 May 2009
Editor: V. Metag

PACS:
25.70.Mn
25.70.De
25.70.-z
25.60.Bx

Keywords:
Exclusive breakup
Sequential peaks
CDCC calculations
Coulomb and nuclear coupling
Correlation asymmetry

ABSTRACT

The exclusive projectile breakup cross section in the ^{6}Li + ^{209}Bi reaction has been measured at $E_{lab} = 40$ and 36 MeV. The sequential breakup, via the resonant state (3^{+}, 2.18 MeV) of ^{6}Li in the continuum, dominates the total $\alpha + d$ breakup. The inclusive breakup α cross section is, however, much larger implying that other competing breakup processes contribute to the α-particle yields. The corrected yields corresponding to two sequential breakup peaks in the α or d spectra were seen to be asymmetric. The average sequential breakup data corresponding to the resonant state are in good agreement with continuum discretized coupled channels (CDCC) calculations. Both Coulomb as well as nuclear field effects were found to be important for the breakup process.

1. Introduction

Projectile dissociation in the field of a target nucleus is a topic of continued interest because of its application to the determination of radiative capture cross section [1] of astrophysical interest. In the absence of nuclear or higher order Coulomb effects on the reaction, the astrophysical S factor can be extracted for low relative energies. Understanding the reaction mechanisms of loosely bound projectiles and the coupling of their breakup on various channels is very important, especially in the context of the increasing number of the radioactive ion beam facilities and the quest for super heavy elements by the fusion of nuclei near the drip line.

Measurements involving the projectiles ^{6,7}Li, ^{6}He with $\alpha + x$ cluster structure show significantly larger cross sections for the inclusive alpha particle production [2–7] compared to the production of the complementary fragment (x). This indicates that there are mechanisms other than $\alpha + x$ breakup responsible for the inclusive production of alpha particles. Exclusive measurements of alpha particles are essential to delineate the different processes leading to such a large inclusive cross section and to understand the effect of projectile breakup on other channels.

The ^{6}Li projectile, while moving in the field of a target nucleus, can dissociate into α and d. This dissociation can either be direct or sequential. In the sequential process, (i) ^{6}Li may first get excited to an inelastic resonant state of finite width or (ii) exchange nucleons with the target before decaying into two breakup fragments in flight. Experimentally, the identification of different breakup processes and the measurement of the exclusive cross sections are challenging tasks.

In this Letter, we present the exclusive measurement of ^{6}Li breakup cross sections exploring the above possibilities. Cross sections for both sequential as well as direct breakup are measured and compared with the continuum discretized coupled channel (CDCC) calculations. The breakup cross sections for different channels along with theoretical calculations have been compared to disentangle the individual contributions to inclusive α production, and get a complete picture of the different reaction mechanisms involved. The measured elastic scattering angular distributions were used as a constraint to the CDCC calculations ensuring that the same set of potential parameters were used to explain both elastic scattering and the breakup process.

2. Experiment and data analysis

The experiment was performed using the ^{6}Li beam from the 14-UD Pelletron in Mumbai at energies 40 and 36 MeV. A self-

* Corresponding author.
E-mail address: ssantra@barc.gov.in (S. Santra).

0370-2693
doi:10.1016/j.physletb.2009.05.016

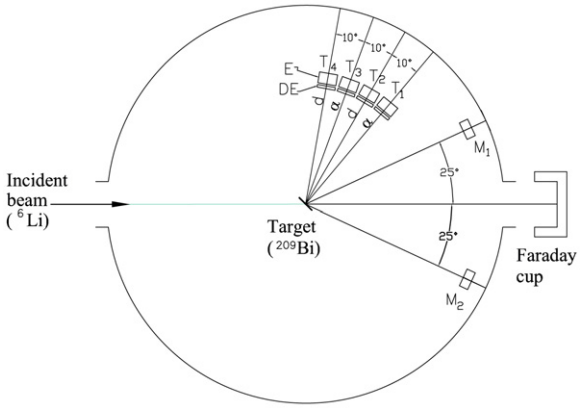

Fig. 1. Schematic of experimental setup for coincidence measurement.

supporting natural Bi target of thickness ≈ 1 mg/cm^2 was employed in the measurement. When the excited ^{6}Li dissociates in-flight into an alpha and deuteron, the fragments are emitted within a cone. The maximum angle [5] between the breakup fragments (α and d) from the decay of ^{6}Li* (3^+, 2.18 MeV) is in the range of $\theta_{\rm lab} = 16°$–$19°$ for the ^{6}Li* angular range of 0°–150°. If the two fragment detectors are kept within this cone, there are two possible directions of the alpha (or deuteron) in the rest frame of ^{6}Li that can reach a specified laboratory angle [8,9] resulting in two peaks in the spectra of alpha (or deuteron). The α and d detectors were kept 10° apart in order to detect each of the breakup fragments with both the peaks arising from sequential breakup corresponding to the above resonant state.

Four telescopes (T_1–T_4) of Si surface barrier detectors were placed inside a 1 m diameter scattering chamber (Fig. 1). Each telescope was provided with a 10 mm diameter collimator to restrict the angular spread to $\pm 1.4°$. The "α-telescopes", T_1 and T_3 were optimized for the detection of particles around $Z = 2$–3 by selecting ΔE detectors of 33 μm thickness and E of 500 μm while the "deuteron-telescopes", T_2 and T_4 with thicknesses $\Delta E = 150$ μm and $E = 1000$ μm were suitable for the detection of particles around $Z = 1$–3. Coincidences between each α- and deuteron-telescope pair (T_1–T_2, T_2–T_3 and T_3–T_4) were ensured by using individual Time to Amplitude Converters (TACs). Two surface barrier detectors (M_1 and M_2) of thickness 2 mm were placed at $\pm 25°$ of the beam for normalization and beam monitoring. The inclusive two-dimensional spectra of ΔE versus E (Fig. 2[a], [d]) showed good separation of particles with different masses.

In the offline analysis, coincidence conditions consisting of two-dimensional gates to select α-particles and deuterons in the corresponding telescopes and a gate around the TAC peak were applied to project inclusive α and d spectra. Fig. 2[a] shows the ungated two-dimensional spectrum in T_1 at $\theta_\alpha = 55°$. After applying the coincidence conditions corresponding to the deuteron telescope at $\theta_d = 65°$ we obtain the projections shown in Fig. 2[b] and [c]. Similarly the two-dimensional spectrum in T_2 at $\theta_d = 65°$ is shown in Fig. 2[d] and gated projections in Fig. 2[e] and [f]. The α and d spectra show two peaks corresponding to sequential breakup. It was observed that the area under the low energy peak in the α spectrum matches with that of the high energy peak in the deuteron spectrum, and vice-versa. A small contribution from direct breakup can also be seen in the region between the two peaks of the spectra.

The experimental data for E_α versus E_d corresponding to the α–d coincidence events at $\theta_\alpha = 55°$, $\theta_d = 65°$ and $E_{\rm lab} = 40$ MeV is shown in Fig. 3[a]. The solid line, represented by "$E_\alpha + E_d = 37.4$ MeV", corresponds to three-body kinematics assuming projectile breakup through its first resonant state (2.18 MeV, $J^\pi = 3^-$)

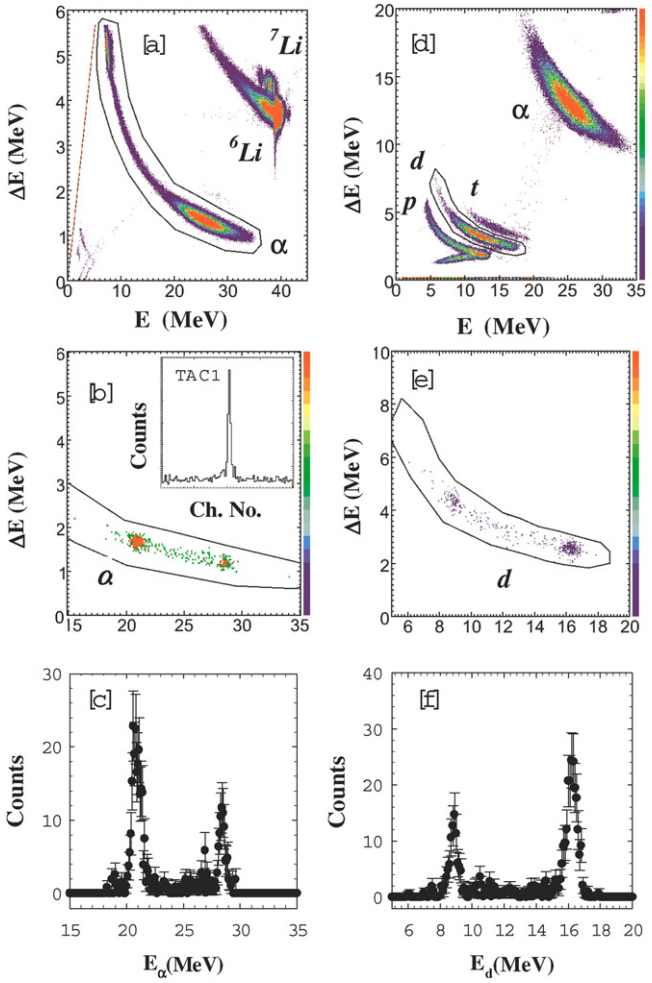

Fig. 2. (Colour online.) Typical two-dimensional (ΔE versus E) spectra acquired in [a] T_1 (at 55°) and [d] T_2 (at 65°) at 40 MeV beam energy. The resulting spectra after applying coincidence conditions are shown in [b], [c] and [e], [f] respectively. One of the TAC spectra used in gating is shown as an inset in [b].

leaving ^{209}Bi target in its ground state. Fig. 3[b] shows the data in terms of α–d relative energy ($E_{\alpha d} = \frac{1}{2}\mu_{\alpha d} v_{\alpha d}^2$) versus alpha particle energy (E_α). When α and d are detected in coincidence at angles θ_α and θ_d respectively, the relative energy is defined as [10],

$$E_{\alpha d} = \frac{1}{(m_\alpha + m_d)}\big[m_d E_\alpha + m_\alpha E_d - 2(m_\alpha m_d E_\alpha E_d)^{1/2} \times (\cos\theta_\alpha \cos\theta_d + \sin\theta_\alpha \sin\theta_d)\big].$$

In this figure two prominent localized contributions corresponding to $E_{\alpha d} = 0.71$ MeV (dotted line) can be seen. From 3-body kinematics [11] (solid line) they were identified as sequential peaks corresponding to the transitions from 1^+, ground state to 3^+, 2.18 MeV resonant state of ^{6}Li which lies above the $\alpha + d$ breakup threshold (1.475 MeV).

It can be seen that the yields of the two peaks corresponding to sequential breakup are unequal. However, a transformation to the centre-of-mass system as described below is necessary before making a conclusion about any asymmetry in the emission of breakup fragments.

The α–d coincidence yields corresponding to the two peaks were used to calculate the differential breakup cross sections in the centre-of-mass system at various angles. In order to do this, we assumed isotropic emission of the breakup fragments in the rest frame of ^{6}Li, and used the formulation of Ref. [10]. The two

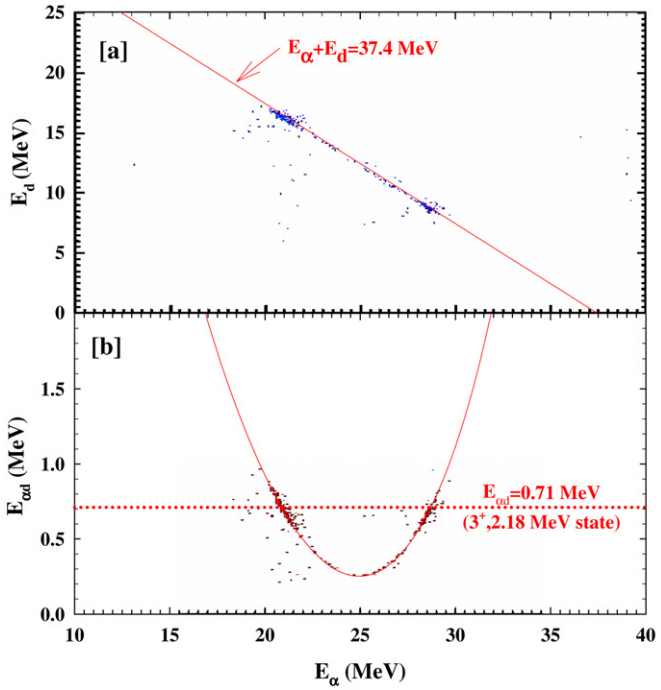

Fig. 3. (Colour online.) The measured α–d coincidence events with $\theta_\alpha = 55^\circ$ and $\theta_d = 65^\circ$ at a beam energy of 40 MeV, shown in scatter plots as [a] E_α versus E_d, and [b] E_α versus $E_{\alpha d}$ (relative energy). The solid lines correspond to the calculation using 3-body kinematics.

peaks in each spectrum correspond to centre-of-mass angles of ^{6}Li* [8,9] which are only slightly different, however the Jacobian factors [11] of the transformation differ considerably. The results are shown in Figs. 4[a] and 5[a] for 40 and 36 MeV respectively. The cross sections obtained using the low (or high) energy peak of α or d detected in an angle forward of its complementary fragment are represented by filled circles (open circles). It can be seen that the differential cross sections represented by solid circles are systematically higher than that represented by open circles. This means that the backward going fragment corresponding to the low energy peak, when detected at an angle forward of its complementary fragment, is always enhanced.

The extraction of differential cross sections assumes isotropic emission of α (and d) in the rest-frame of ^{6}Li. This is what one would *a priori* expect. However, the results of Figs. 4[a], 5[a] show that there is a forward–backward asymmetry. In view of the limited coverage of the 4π solid angle in the coincidence data, a rigorous extraction of cross sections is not possible. However, the average of the cross sections obtained from the two peaks is probably a good representation. The possible reasons for asymmetry are discussed in Section 4.

In Figs. 4[b] and 5[b] we also show the elastic scattering angular distribution data (filled squares) which were simultaneously explained by the coupled channel calculation.

In addition to sequential breakup, the differential cross sections for direct breakup were extracted considering relative energies, $E_{\alpha d}$ from the minimum ($\sim$0.25 MeV) upto 0.71 MeV excluding the contributions from the peaks attributed to sequential breakup.

For each angle-set of α and d detectors there is a minimum relative energy $E^{\min}_{\alpha d}$ below which the coincidence particles cannot be detected. The energies of α and d corresponding to these $E^{\min}_{\alpha d}$ were calculated from 3-body kinematics. Two sets of direct breakup cross sections were obtained by integrating the coincidence yields between this minimum and the two sequential peaks in either direction. The average of the two direct breakup cross sections obtained for each angle set are shown as filled diamonds

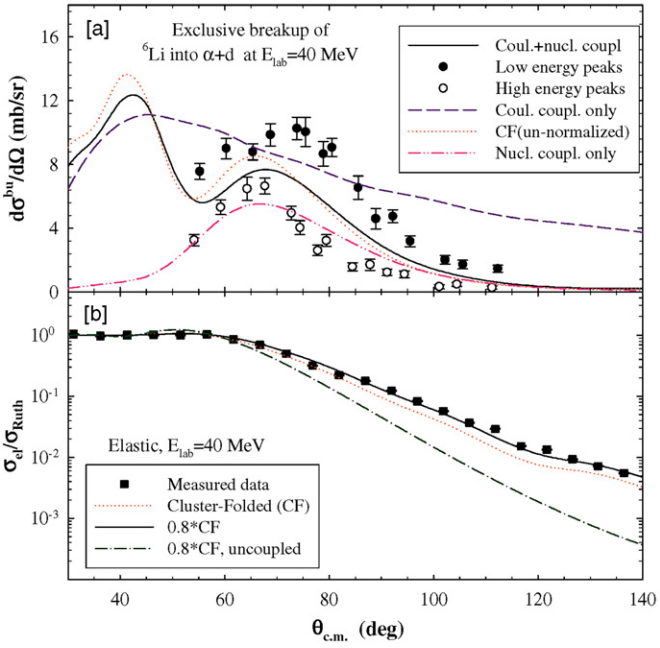

Fig. 4. (Colour online.) [a] Exclusive breakup cross section in centre-of-mass frame measured at 40 MeV. Filled (open) circles represent the cross sections obtained using the bigger (smaller) peaks of the two sequential breakup peaks. Solid, dashed and dashed-dot-dot lines represent the result of CDCC calculations with Coulomb + nuclear, only Coulomb and only nuclear coupling respectively. Dotted line represents the calculation with un-normalized CF potential. [b] Elastic scattering angular distribution at $E_{lab} = 40$ MeV. The results of CDCC calculation with full couplings and normalized (un-normalized) cluster-folded potential is represented by solid line (dotted line). Dashed-dot line was obtained with normalized CF potential but without any breakup coupling.

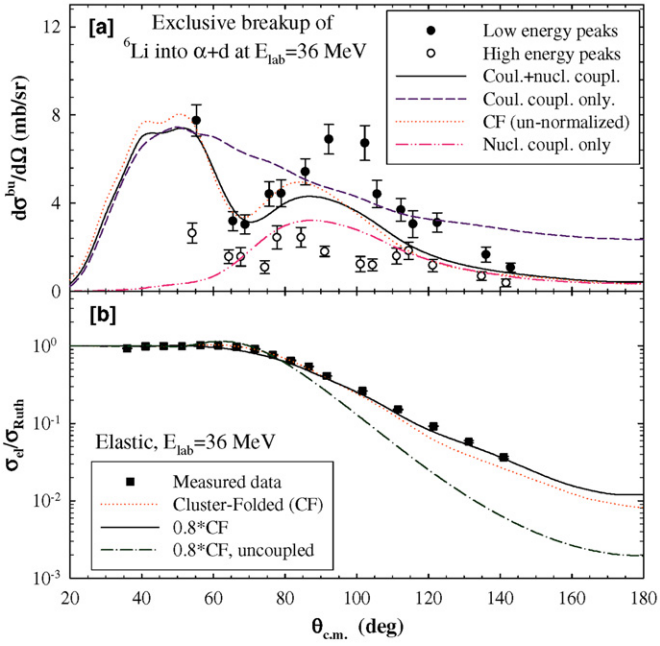

Fig. 5. (Colour online.) Same as Fig. 4 but for 36 MeV.

in Fig. 6. Filled circles represent the average sequential $\alpha + d$ breakup cross section obtained from the two sequential peaks. The data reveals that direct breakup for the present beam energies is smaller by about one order of magnitude compared to sequential breakup.

To compare the sequential $\alpha + d$ breakup cross sections with the total α-production due to breakup [5], the inclusive α cross

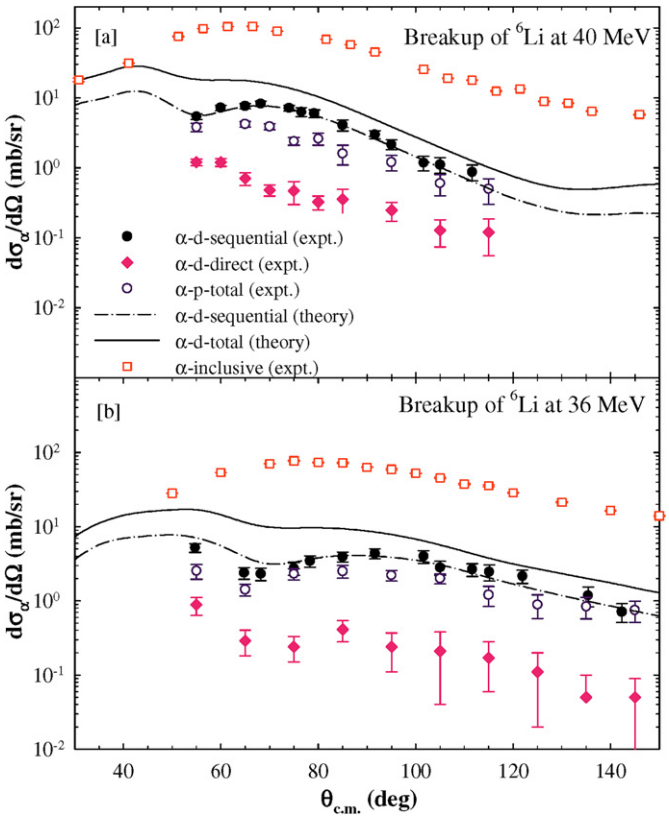

Fig. 6. (Colour online.) Cross sections for inclusive α production (open squares) and exclusive projectile breakup ($^6\mathrm{Li} \rightarrow \alpha + d$ and $^6\mathrm{Li} \rightarrow \alpha + p + n$) (see text for details).

sections were extracted and shown as open squares in Fig. 6. It can be seen that the average sequential $\alpha + d$ breakup cross sections (filled circles) obtained from low and high energy peaks are about one order of magnitude less than the inclusive α breakup production. While searching for other possible sources of α-production, it was observed that a large fraction of α counts in the spectra of T_1 (T_3) were produced in coincidence with protons detected in T_2 (T_4). As observed in Ref. [8], this is mostly due to $1n$ transfer ($^6\mathrm{Li} + {}^{209}\mathrm{Bi} \rightarrow {}^5\mathrm{Li} + {}^{210}\mathrm{Bi} + Q_{opt}$) followed by breakup of ^{5}Li ($\rightarrow \alpha + p + 1.97$ MeV). The probability of (i) breakup of $^6\mathrm{Li} \rightarrow \alpha + p + n$ with a Q-value of -3.7 MeV, or (ii) ^{6}Li first dissociating into $\alpha + d$ and then d breaking into $p + n$ is estimated to be small by Q-value considerations. Breakup cross sections for $\alpha + p$ channel were deduced from the data (open circles in Fig. 6), and it can be seen that they are much higher than the direct and comparable to the sequential $\alpha + d$ breakup. Similar results (i.e., transfer followed by breakup, $^7\mathrm{Li} \rightarrow {}^6\mathrm{Li}^* \rightarrow \alpha + d$) have been observed for $^7\mathrm{Li} + {}^{65}\mathrm{Cu}$ system [12].

3. Coupled channel calculations for ^{6}Li breakup

The CDCC method was used to calculate the cross sections for elastic and breakup channels with the code FRESCO [13]. ^{6}Li was taken as a cluster of $\alpha + d$ for its bound as well as continuum states. The breakup of the projectile into its fragments (α and d) is considered to be caused by inelastic excitations to different partial waves in the continuum, induced by interactions of the projectile fragments with the target by Coulomb as well as nuclear forces. For ^{6}Li, couplings to the 3^+ ($E_x = 2.18$ MeV), 2^+ ($E_x = 4.31$ MeV), and 1^+ ($E_x = 5.65$ MeV) resonant states as well as couplings to the non-resonant continuum were included. The continuum up to an excitation energy of 8 MeV with α–d relative momentum $L = 0$, 1 and 2 was included in the coupling. For s and p waves, the continuum was discretized into 16 bins of equal width in the momentum of αd relative motion. In the presence of resonances for d-waves, the discretization of the continuum was slightly modified in order to avoid double counting. Three resonant states, with widths corresponding to 0.1 MeV, 2.0 MeV and 3.0 MeV, respectively, were also treated as momentum bins, but with finer steps.

The couplings of the ground state to the continuum as well as continuum to continuum have been included. Reorientation coupling, i.e., the coupling of the quadrupole term of the projectile fragment-target potentials was also incorporated. Since the inelastic cross section corresponding to the target excitation was found to be very small, and the effect of its coupling on the elastic is known to be insignificant [14], no target excitation was included in the CDCC calculation. The effect of the target spin on other channels being negligible, the spin was taken to be zero, in order to reduce the computation time.

The CDCC calculations were performed using cluster-folded (CF) interaction [15], where α-target ($V_{\alpha+\mathrm{Bi}}$) and deuteron-target ($V_{d+\mathrm{Bi}}$) optical potentials were evaluated at $E_\alpha \approx \frac{2}{3}E_{6\mathrm{Li}}$ and $E_d \approx \frac{1}{3}E_{6\mathrm{Li}}$, respectively. Once a certain set of potential parameters for $V_{\alpha+\mathrm{Bi}}$ and $V_{d+\mathrm{Bi}}$ are chosen, there is no free parameter remaining in the model, except a possible overall renormalization factor [16]. The $V_{\alpha+\mathrm{Bi}}$ potential used in our calculations was taken from Ref. [17] for $E_{\mathrm{lab}} = 24.8$ MeV. Both the real and the imaginary potentials were of Woods–Saxon volume form and the parameters are: $v_0 = 85.94$ MeV, $r_0 = 1.361$ fm, $a_0 = 0.578$ fm, $w = 13.5$ MeV, $r_w = 1.412$ fm, $a_w = 0.299$ fm. Similarly, the $V_{d+\mathrm{Bi}}$ potential, with real parameters $v_0 = 80.2$ MeV, $r_0 = 1.15$ fm, $a_0 = 0.973$ fm, and imaginary parameters $w = 15.37$ MeV, $r_w = 1.45$ fm, $a_w = 0.559$ fm, was taken to be same as that of $d + {}^{208}\mathrm{Pb}$ at 12 MeV [18]. Imaginary parts of $V_{\alpha+\mathrm{Bi}}$ and $V_{d+\mathrm{Bi}}$ describe the removal of flux whenever the individual fragments themselves breakup, excite, or fuse with the target. The strength of the real part of $V_{\alpha+\mathrm{Bi}}$ as well as $V_{d+\mathrm{Bi}}$ was scaled by a factor of 0.8, compared to the values in Refs. [17,18], in order to explain the elastic data for both 40 and 36 MeV (see Figs. 4[b] and 5[b]).

The $\alpha + d$ binding potential in ^{6}Li was also of Woods–Saxon shape and the parameters were taken to be the same as in Ref. [19]. Two separate potentials were used for (i) ground state and s-wave continuum and (ii) p- and d-wave continuum. These potentials were chosen as they reproduce the resonances (energies and widths) correctly [20], and particularly the d-wave resonance whose breakup contribution is maximum as observed in our experimental data.

Coupled channels calculations with the above potentials were performed with different couplings, at two energies: $E_{\mathrm{lab}} = 40$ and 36 MeV. In Figs. 4[b] and 5[b], the elastic scattering angular distribution data (filled squares) are compared with the calculations. A comparison of the solid line (full couplings) with the dashed-dot line (no couplings) shows that the coupling of the breakup channels has a very large effect on elastic scattering. The dotted line represents the calculation using un-normalized CF potential generated directly from the parameters of Refs. [17] and [18]. The CF potential with its real part normalized by a factor of 0.8 gave a better fit to the elastic scattering angular distributions at both the energies, and hence the remaining calculations were done using normalized CF potential. Since, the elastic cross section obtained with full couplings reproduces the experimental data reasonably well, it ensures that the optical potentials for fragment-target interactions used in the CDCC calculations to obtain the cross sections for the elastic and the breakup channels simultaneously are not arbitrary.

The breakup cross sections calculated for the d-waves with $J^\pi = 3^+$ channel have been compared with the experimental data in Figs. 4[a] and 5[a]. The calculations with Coulomb coupling,

Table 1
Experimental and calculated cross sections for various channels at $E_{lab} = 40$ and 36 MeV.

Reaction channel	σ_{40}(mb)		σ_{36}(mb)	
	(expt)	(cal)	(expt)	(cal)
Inclusive breakup-α	500 ± 25	–	493 ± 20	–
^{6}Li*$(3^+) \rightarrow \alpha + d$ (sequential)	50 ± 5	50	44 ± 4	43
^{6}Li* $\rightarrow \alpha + d$ (direct)	7.5 ± 2.0	23	3.5 ± 1.2	15
^{6}Li* $\rightarrow \alpha + d$ (total)	–	113	–	94
^{6}Li* $\rightarrow {}^5$Li $\rightarrow \alpha + p$	27.5 ± 5.0	–	26 ± 4.5	–
Incomplete fusion	235 ± 11[a]	238	165 ± 10[a]	174
Complete fusion	558 ± 18[a]	601	345 ± 5[a]	345
Reaction	1013 ± 40	1153	910 ± 32	809

[a] Ref. [21].

nuclear coupling and Coulomb + nuclear coupling are shown as dashed, dashed-dot-dot and solid lines respectively. It was found that the breakup cross sections calculated with Coulomb + nuclear couplings are in between the two sets of data obtained using the low- and high-energy peaks of the sequential breakup. One can see that nuclear coupling is necessary in order to explain the data particularly at the backward angles, making its effect very prominent. Calculations with only nuclear coupling (dashed-dot-dot line) reveal that, at these energy and angular range of data, there is a substantial contribution to breakup from nuclear interaction.

To understand the various exclusive breakup contributions to the inclusive breakup α spectra, the CDCC results are compared in Fig. 6. It can be seen that the calculated cross sections (dashed-dot line) for α–d breakup via 3^+ resonant state of ^{6}Li reproduces the average experimental data quite well. The total α–d breakup (solid lines) for both the resonant and the non-resonant continuum, calculated up to an excitation energy of 8 MeV (which also includes the undetected α–d breakup contribution), was found to be far less than the inclusive α. The experimental α–p breakup together with the total theoretical α–d breakup cannot account for the large difference between exclusive and inclusive data, especially near and above the grazing angle. It may be mentioned that the measured α–p breakup using the present detector configuration does not cover the whole range of relative momentum. The other possible sources of alpha are (i) (^{6}Li, ^{5}He) reaction followed by breakup of $^5\text{He} \rightarrow \alpha + n$, (ii) (^{6}Li, ^{7}Li) reaction followed by breakup of $^7\text{Li} \rightarrow \alpha + t$, (iii) (^{6}Li, ^{4}He) reaction at optimum Q-value and (iv) partial fusion of the complementary breakup fragment i.e., deuteron. The cross sections for (^{6}Li, ^{5}He) and (^{6}Li, ^{4}He) reactions were calculated and found to be negligible (<1 mb). Though the cross section for (^{6}Li, ^{7}Li) reaction was found to be substantial (∼10 mb) from both calculation as well as experiment, the breakup cross section of $^7\text{Li} \rightarrow \alpha + t$ was found to be negligible from the present experimental data. However, the incomplete fusion (ICF) for the present system was already measured [21] to be a large fraction (≈ 40–50%) of complete fusion at these energies. So, it is possible that a large fraction of the missing contribution in inclusive α is from the last process (iv). A 3-dimensional classical trajectory model calculation [22] has been made to estimate the cross section for the incomplete fusion. The model parameters were chosen so as to reproduce the complete fusion data. The results are in good agreement with the data in the literature. A comprehensive list of all the cross sections are given in Table 1. The sum of the measured cross sections for CF, ICF, breakup ($\alpha + d$ and $\alpha + p$) and 1n pickup reactions is ≈ 889 mb and ≈ 630 mb at 40 and 36 MeV respectively, which exhausts ∼80% of the total experimental reaction cross section. The rest of the reaction cross section must be accounted for by the undetected breakup channels and other transfer channels.

4. Asymmetry in resonant breakup peaks

A systematic difference in the experimental cross sections estimated from low- and high-energy peaks corresponding to the sequential breakup was observed in the present data. In particular, it was observed that the Jacobian corrected yield of the low energy peak of any particle detected at an angle forward of its complementary fragment is always enhanced. This is contrary to what would be expected if breakup is isotropic in the rest frame of ^{6}Li.

Asymmetry in the yields of the two peaks has also been observed previously [6,23,24]. Gupta et al. in their data on $^7\text{Li} + {}^{58}\text{Ni}$ [24], found that the high energy triton (or low energy α) is favoured compared to its counterpart. However in this case the triton detector was placed forward of the α detector, in contrast to the present observation. Shotter et al. [23] in their measurements on $^7\text{Li} + {}^{208}\text{Pb}$, kept the α- and d-detectors in a vertical geometry, with the one telescope above and the other below the reaction plane. They observed that the low energy tritons were enhanced which was opposite to the observation of Gupta et al. Thus, the origin of asymmetry could be different depending on the projectile-target combination.

Orientation effects and final state interactions between the fragments and the target, and among the fragments themselves, are known to distort the energy spectra and modulate detector efficiency [25]. However, for sequential breakup of ^{6}Li via the 3^+ state, the long lifetime ($\Gamma \approx 24$ keV; $\tau \sim 2.8 \times 10^{-20}$ s) leads to dissociation far (∼180 fm) from the target, where the final state interactions should be weak.

Another possible reason for the observed asymmetry could be a shift of the direct breakup yield into the region of the sequential breakup peaks. Direct breakup occurs close to the target and a shift in energy could arise from differences in the Coulomb induced post-breakup acceleration of the fragments [25]. However, breakup of ^{6}Li results in fragments α and d which have the same Z/A ratio and hence no difference in post-acceleration. We therefore do not expect a contribution to the sequential breakup peaks from direct breakup in this case.

The main reason for the asymmetry appears to be the anisotropic distribution of the breakup fragments in the rest frame of ^{6}Li. This could arise from the strong polarization of the clustered ^{6}Li in the target field as mentioned in Ref. [9,26]. Another possible factor is the reorientation effect due to the static quadrupole moment of the 3^+ state [26]. Since the 3^+ state corresponds to $\ell = 2$ (d-state), emission of α and d in the rest frame of ^{6}Li would not be isotropic.

5. Summary and conclusions

The cross sections for exclusive and inclusive breakup of the projectile along with elastic scattering for $^6\text{Li} + {}^{209}\text{Bi}$ system have been measured at 40 and 36 MeV. Sequential breakup of ^{6}Li via the resonant state (3^+) of ^{6}Li in the continuum, dominates the total $\alpha + d$ breakup cross section at these two energies. Two sequential breakup peaks, in both alpha and deuteron spectra, arising due to forward and backward going breakup fragments were found to be asymmetric, and give rise to different cross sections in the centre of mass frame. CDCC calculations have been performed with the cluster folded potential, using the elastic scattering data to constrain the potential parameters. The $\alpha + d$ breakup cross sections calculated using the CDCC method agrees with the average of the two sets of experimental data that are obtained from the two sequential breakup peaks. The calculations reveal that the breakup data, particularly at backward angles, can be explained only by Coulomb + nuclear coupling.

The cross sections measured for $^{6}\mathrm{Li} \rightarrow {}^{5}\mathrm{Li} \rightarrow \alpha + p$ channel, i.e., transfer followed by breakup, was found to be comparable to resonant breakup via 3^{+} of $^{6}\mathrm{Li}^{*}$ and much higher than non-resonant $\alpha + d$ breakup. The exclusive breakup cross sections for these channels along with the CDCC calculations have been compared in Fig. 6 to disentangle their individual contributions in inclusive α breakup, and to get a complete picture of the reaction mechanisms involved. A large difference was observed between the sum of exclusive and inclusive breakup α cross sections. The rest of the inclusive α is possibly due to the partial fusion of the complementary breakup fragment i.e., deuteron. This is supported by the fact that the measured [21] as well as calculated incomplete fusion for the present system is a large fraction ($\approx$ 40–50%) of complete fusion at these energies.

A systematic difference in experimental cross sections estimated from low- and high-energy sequential peaks observed in the present data implies that one should be careful while estimating the cross sections from any one sequential peak and deriving any conclusion by comparing with the calculations. Understanding the origin and estimating the extent of the asymmetry reported in the present work remains an open question.

References

[1] G. Baur, et al., Nucl. Phys. A 458 (1986) 188.
[2] A. Pakou, et al., Phys. Rev. Lett. 90 (2003) 202701.
[3] G.R. Kelly, et al., Phys. Rev. C 63 (2000) 024601.
[4] A. di Pietro, et al., Europhys. Lett. 64 (2003) 309.
[5] C. Signorini, et al., Phys. Rev. C 67 (2003) 044607.
[6] C.M. Castaneda, et al., Phys. Lett. B 77 (1978) 371.
[7] H. Utsunomiya, et al., Phys. Rev. C 28 (1983) 1975.
[8] C.M. Castaneda, et al., Phys. Rev. C 21 (1980) 179.
[9] D. Scholz, et al., Nucl. Phys. A 288 (1977) 351.
[10] R.J. de Meijer, R. Kamermans, Rev. Mod. Phys. 57 (1985) 147.
[11] H. Fuchs, Nucl. Instrum. Methods 200 (1982) 361.
[12] A. Shrivastava, et al., Phys. Lett. B 633 (2006) 463.
[13] I.J. Thompson, Comput. Phys. Rep. 7 (1988) 167.
[14] K. Rusek, et al., Nucl. Phys. A 614 (1997) 112.
[15] F.G. Perey, G.R. Satchler, Nucl. Phys. A 97 (1967) 515.
[16] Y. Hirabayashi, Y. Sakuragi, Phys. Lett. B 258 (1991) 11.
[17] P. Singh, et al., Phys. Rev. C 43 (1991) 1867.
[18] P.R. Christensen, et al., Nucl. Phys. A 129 (1969) 337.
[19] H. Nishioka, et al., Nucl. Phys. A 415 (1984) 230.
[20] A. Diaz-Torres, et al., Phys. Rev. C 68 (2003) 044607.
[21] M. Dasgupta, et al., Phys. Rev. C 70 (2003) 024606.
[22] A. Diaz-Torres, et al., Phys. Rev. Lett. 98 (2007) 152701.
[23] A.C. Shotter, et al., Phys. Rev. Lett. 46 (1981) 12.
[24] D. Gupta, et al., Nucl. Phys. A 646 (1999) 161.
[25] J.E. Mason, et al., Phys. Rev. C 45 (1992) 2870.
[26] D.L. Disdier, et al., Phys. Rev. Lett. 27 (1971) 1391.